Available online at www.sciencedirect.com
SCIENCE DIRECT
Journal of Molecular Spectroscopy 238 (2006) 213–223
Journal of MOLECULAR SPECTROSCOPY
www.elsevier.com/locate/jms

The $B\ ^3\Sigma^-$ state of the SO radical

Ching-Ping Liu [a], Nicola L. Elliott [b], Colin M. Western [b,*], Yuan-Pern Lee [a,c], Reginald Colin [d]

[a] Department of Applied Chemistry and Institute of Molecular Science, National Chiao Tung University, Hsinchu 30010, Taiwan
[b] School of Chemistry, University of Bristol, BS8 1TS, UK
[c] Institute of Atomic and Molecular Sciences, Academia Sinica, Taipei 10617, Taiwan
[d] Laboratoire de Chimie Quantique et Photophysique, Université Libre de Bruxelles, Brussels, Belgium

Received 9 April 2006; in revised form 8 May 2006
Available online 12 May 2006

Abstract

Spectra of the $B\ ^3\Sigma^- - X\ ^3\Sigma^-$ transition in SO above the first dissociation limit are recorded using degenerate four wave mixing. These spectra are combined with earlier work involving laser induced fluorescence, absorption spectra and Fourier transform emission spectra, to enable a rotational analysis and deperturbation of vibrational levels of the B state up to $v' = 16$. Numerous perturbations were noted within the $B\ ^3\Sigma^-$ state, and the origin of these is discussed. In a number of cases, these perturbations can be attributed to interactions with specific other electronic states of SO, such as $A\ ^3\Pi$, $C\ ^3\Pi$, $d\ ^1\Pi$, and $A''\ ^3\Sigma^+$.

Keywords: SO; Radicals; DFWM; Perturbations; Electronic spectroscopy

1. Introduction

The $B\ ^3\Sigma^- - X\ ^3\Sigma^-$ transition dominates the absorption spectrum of SO between 41 000 and 52 000 cm^{-1}. The first major work on the electronic spectroscopy of SO was Martin's study of this B–X transition [1], which recorded emission spectra from the $v' = 0$, 1, 2, and 3 levels of the B state in a discharge tube. Predissociations within these first four vibrational levels were noted, and were attributed to a crossing with a $^3\Pi$ state. A number of further flash photolysis studies of the B–X transition, this time in absorption, extended the coverage of the B state to what appears to be $v' = 30$, close to the dissociation limit [2–4]. Variations in the level of diffuseness of the vibrational bands indicated additional predissociation mechanisms, around $v' = 14$ and $v' = 17$. Later, the high-resolution Fourier transform emission spectra of Clerbaux and Colin [5] enabled analysis of the B–X transition to be carried out in much greater detail for levels below the dissociation limit. The rotational structure of the $v' = 0$ and $v' = 1$ levels was analysed, and a set of molecular constants for these two B state vibrational levels was obtained. Based on the N dependence of the break off in emission in $v' = 0$–3 the first dissociation limit was determined to be at 43 680 cm^{-1}.

All these studies indicated various perturbations in most, if not all, the vibrational levels of the B state, though a detailed analysis of the origin of these irregularities was not possible. Perturbations were very evident in the flash photolysis absorption spectra recorded by Colin, although only a limited amount of rotational analysis was possible due to the resolution of these spectra. Clerbaux and Colin identified several irregularities in the rotational structure of $v' = 0$ and $v' = 1$ although again, no suggestions as to the cause of these perturbations were made.

This work provides a more complete rotational analysis and deperturbation of vibrational levels within the $B\ ^3\Sigma^-$ state of SO, by combining new experimental measurements with previous data. A range of techniques were employed to obtain absorption and emission spectra of the $B\ ^3\Sigma^- - X\ ^3\Sigma^-$ transition. These included degenerate four wave mixing (DFWM), laser induced fluorescence (LIF), photo-

* Corresponding author. Fax: +44 0 117 925 1295.
E-mail address: C.M.Western@bristol.ac.uk (C.M. Western).

0022-2852/$ - see front matter © 2006 Elsevier Inc. All rights reserved.
doi:10.1016/j.jms.2006.05.005

graphic plate absorption, and Fourier transform emission spectroscopy. Combining a range of spectra, taken under different conditions using different techniques, has provided the information necessary for the analysis of the more perturbed vibrational levels of the B state, and in some cases allows us to see the perturbing states directly.

More recent work on other electronic states of SO has enabled the source of several B state perturbations to be identified here. There are a number of electronic states of SO which are known to be candidates for perturbation of the B state; a potential energy diagram showing all the known bound states in the region is shown in Fig. 1. As the lowest levels of the B state are just below the first dissociation limit, any state correlating with this limit can interact with the B state. Of these, only the $A\ ^3\Pi$ state has been reasonably well characterised up to the dissociation limit [6]. The ground state ($X\ ^3\Sigma^-$) and the lowest lying excited states, $a\ ^1\Delta$ and $b\ ^1\Sigma^+$, have been well characterised by microwave [7] and infra-red [8–10] studies, and the Fourier transform emission study [5] of the B–X transition provided information up to $X\ v'' = 21$; however, none of this work extends all the way up to the dissociation limit. There are also a number of other states, which are known to be bound, but about which very little information is available. The $c\ ^1\Sigma^-$ state has been observed in Ar and Ne matrices [11], and more recently in emission in the gas phase [12], but these experimental data are limited. Similarly, little is known of the $A''\ ^3\Sigma$ state, although it has also been observed in emission [13]. Apart from matrix work [11], there is only indirect experimental evidence of the $A'\ ^3\Delta$ state [14] and even less is known of the bound $^5\Pi$ state shown in Fig. 1, which has only been postulated from theoretical calculations [15]. SO is unusual in that two bound states, the $C\ ^3\Pi$ and $d\ ^1\Pi$ states, have been found just above the dissociation limit [15], using $1 + 1$ multiphoton ionisation spectroscopy. The d state was found to be weakly bound, with the highest level being $v' = 3$; the C state supports significantly more vibrational levels although only $v' = 0$ and $v' = 1$ have been observed experimentally. Theoretical calculations on the C state [15,16] show that it undergoes an avoided crossing with a repulsive state at $r \approx 2.05$ Å; this can be seen in Fig. 1. Note that Fig. 1 includes RKR curves derived from experimental data (solid lines) and the results of high level ab initio calculations (dashed lines) from references [15,16] supplemented by a few calculations described in the text below.

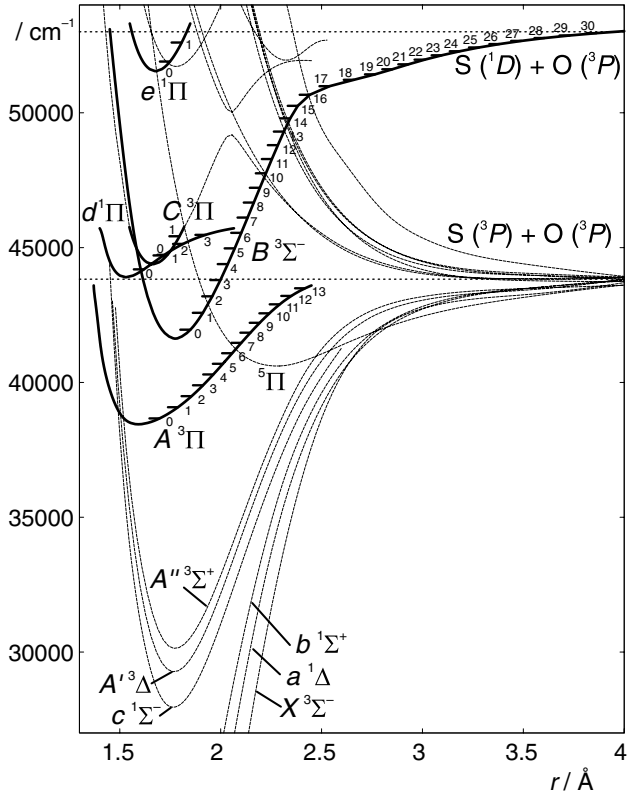

Fig. 1. Overall potential energy diagram showing all currently known states of SO below 55000 cm^{-1}. The solid lines are generated from RKR curves; the dashed lines are based on high level (MRCI) ab initio calculations.

In this paper, we extend the detailed rotational analysis of the B state to a much wider range of vibrational levels, which allows us to identify some specific interactions of other electronic states with the $B\ ^3\Sigma^-$ state, and perform a deperturbation for selected cases. Interactions involving $A\ ^3\Pi$, $C\ ^3\Pi$, $d\ ^1\Pi$, and $A''\ ^3\Sigma^+$ are discussed, though it is without question that some, if not all, of the other electronic states shown in Fig. 1 will also interact with the B state. A greater understanding of the interactions between $B\ ^3\Sigma^-$ and its nearby electronic states enables a clearer picture of the spectroscopy of SO to be formed.

2. Experimental

This paper presents new spectra of SO, mainly degenerate four wave mixing spectra taken in Taiwan. The analysis also included spectra from previous work recorded using a number of different techniques, which are also described briefly in this section.

2.1. Degenerate four wave mixing

A SO_2/He mixture was prepared in a stainless steel reservoir before expansion through a pulsed nozzle (General Valve, orifice diameter 1 mm); the reservoir was filled with SO_2 to a pressure of 300 Torr near 296 K and diluted with ultrahigh purity helium to a total pressure of 3000 Torr. The pulsed nozzle was operated at 10 Hz with an opening period of 0.50 ms. The stagnation pressure was typically 1.3 atm. SO radicals were produced from the photolysis of SO_2 with an ArF excimer laser (Lambda Physik, LPX 120i or GAM laser, EX100H) operating at 193 nm. The photolysis laser beam was slightly focused several nozzle diameters downstream from the orifice.

The degenerate four-wave mixing (DFWM) experiments are similar to those described previously for two-colour resonant four-wave mixing (TC-RFWM) experiments, but here only one laser was used [17,18].

The frequency-doubled output from a dye laser (Lambda Physik, Scanmate 2E, using dyes LC4200, LC4400, LC4800, LC5000, and selected mixtures) pumped with a XeCl excimer laser (Lambda Physik, LPX 105) at 308 nm is split into three beams of comparable intensities to provide excitation in a spectral region of 214–263 nm. Light from the dye laser had spectral widths $\sim$0.1 cm^{-1} for the fundamental output. Typically 50–150 μJ of laser energy and a beam diameter of $\sim$1.5 mm was used.

The three laser beams of the same polarization propagate in the same direction and cross at small angles ($\sim$1°) 3 mm downstream from the nozzle. The resultant signal beam is allowed to travel 2–3 m through several irises before being spatially filtered with an iris, a convex lens ($f = 10$ cm) and a pinhole (diameter 0.15 mm) in combination, and detected with a photomultiplier tube (Hamamatsu, R955P). The signal was integrated with a gated-integrator (Stanford Research, SR250) and processed with a computer. A digital pulse generator (Stanford Research, DG535) served to control the timing between the pulsed nozzle, the laser system, and the boxcar integrator. The delay between the photolysis and DFWM laser pulses, typically 0.7–2 μs, was adjusted to optimize the signal. Wavelength calibration of the dye laser was achieved either with a Fe–Ne optogalvanic cell or a wavemeter (Burleigh WA-5500, accuracy 0.2 cm^{-1}). DFWM spectra to $v' = 3$–9 of the B–X transition of SO were recorded. Transitions observed using DFWM mostly originated from the $v'' = 2$ level of the X state, due to the non-Boltzmann distribution of SO produced from the SO_2 photolysis [19]. The rotational temperature could be adjusted by adjusting the experimental geometry, with values around 100 K being typical. Note that the DFWM signal depends on the square of the molecular density and the cube of the laser intensity but no attempt was made to normalize the spectra with respect to the intensity of the dye laser and we did not check for saturation effects. This is sufficient for the analysis presented in this work which only requires accurate peak positions. Peak intensities were only used as a rough guide to assignment.

2.2. Laser induced fluorescence

In addition to DFWM spectra, a number of laser induced fluorescence (LIF) spectra were recorded. LIF spectra, covering B $v' = 0$–3, were recorded in Taiwan in conjunction with the DFWM spectra, using the same apparatus and method of radical production; a second photomultiplier was placed near the jet to detect fluorescence in a direction perpendicular to the photolysis beam. As for the DFWM spectra, these showed a rotational temperature of $\sim$100 K. LIF spectra of the B–X transition had also been previously recorded as part of the work by Archer et al. [15]. These spectra were included in analysis of the lower vibrational levels, since their lower rotational temperature ($\sim$15 K) enabled transitions at low J to be easily assigned. In addition, a few selected LIF spectra of B–X hot bands were recorded in Bristol, using essentially the same experimental set-up as described by Archer et al. A molecular iodine spectrum was recorded simultaneously, allowing a detailed check on the overall calibration accuracy. An increased laser power was used in the recording of these spectra, which enabled transitions directly to some perturbing states to be observed alongside the B–X transitions.

2.3. Fourier transform emission spectrum

The analysis also used a Fourier transform emission spectrum of a microwave discharge in an $SO_2 + O_2 + He$ mixture, recorded by Clerbaux and Colin [5]. As it was an emission spectrum, it only included transitions from the $v' = 0$–3 vibrational levels in the B state below the dissociation limit, but included a wide range ($v'' = 0$–21) of vibrational levels in the ground state. The effective temperature ($\sim$1400 K) was much higher than the laser spectra described above, though the resolution was similar (0.2 cm^{-1}).

2.4. Absorption spectra

The last set of spectra covering the B–X transition was a series of flash photolysis absorption spectra. These were recorded on photographic plates and covered almost the entirety of the $B\ ^3\Sigma^- – X\ ^3\Sigma^-$ transition (from $v' = 4$ up to the dissociation limit at approximately $v' = 30$), which were recorded in Ottawa by Colin [4]. To assist in assignment, these photographic plate spectra were transformed into trace spectra using the PGOPHER program [20], though line positions were taken from original measurements from the photographic plates. As for the Fourier transform spectrum, the effective temperature was high ($\sim$700 K), though the resolution was significantly lower (2 cm^{-1}).

2.5. 1 + 1 Multiphoton ionisation spectra

The final source of data used for analysis was a set of $1 + 1$ multiphoton ionisation (MPI) spectra recorded in Bristol [15], covering a range of transitions to the $A\ ^3\Pi$, $C\ ^3\Pi$, and $d\ ^1\Pi$ states. Although these did not provide direct information on the $B\ ^3\Sigma^-$ state, they proved vital in the identification of the source of a number of perturbations seen within the B state.

2.6. Ab initio calculations

High level ab initio calculations were available as described in references [15,16], but to obtain full coverage of the quintet states and repulsive curves we undertook some additional calculations. These were MRCI calculations using an AVQZ basis set with the MOLPRO package [21] and were of similar quality to the previous calculations. In common with the previous results they gave excellent results (in comparison to the RKR curves)

for bond lengths < 2.3 Å, but required empirical shifts of up to 2000 cm^{-1} for longer bond lengths to give the dissociation limits at the right energy.

3. Analysis

The basic principle of analysis was the same for all levels, perturbed or otherwise. A conventional linear molecule Hamiltonian was used

$$\hat{H} = T_v + A\hat{\boldsymbol{L}}\cdot\hat{\boldsymbol{S}} + B\hat{\boldsymbol{N}}^2 + \tfrac{2}{3}\lambda(3\hat{S}_z^2 - \hat{\boldsymbol{S}}^2) + \gamma\hat{\boldsymbol{N}}\cdot\hat{\boldsymbol{S}} + 1/2o(\hat{S}_+^2 e^{-2i\phi} + \hat{S}_-^2 e^{+2i\phi}) \quad (1)$$

to model the X, B, A, C, and d states, with terms omitted as appropriate. The PGOPHER program [20] was then used to simulate and fit the observed spectra. The X state constants were fixed according to those determined by Clerbaux and Colin [5] using a combination of millimeter, IR, and UV data. The energies are defined such that $T_v = 0$ for $v'' = 0$ of the X state, giving the lowest level, ($J = 0$, $v'' = 0$) at -5.59 cm^{-1}. To assign the spectra, a rough simulation was constructed, using these known X state constants and any available constants for the B state (and other states, where appropriate). Assignment of rotational lines in the rough simulation to those in the experimental spectra was then possible, particularly given that accurate ground state common differences could be used to confirm the assignments. To model perturbations, the PGOPHER program was set up to include all the interacting states in a single Hamiltonian matrix, with matrix elements as described later for the individual interactions. Finally, a least-squares fit was carried out to obtain revised values for the constants for the B state and the states interacting with it. It is well known that the lineshapes and intensities of DFWM spectra are complicated to model, but we found that simply squaring the intensities was sufficient for our analysis. The observed lineshapes were symmetrical, and common differences confirmed that there were no significant peak shifts in the DFWM spectra.

We illustrate the analysis by discussing selected bands below. Files containing observed and calculated positions for each of the fits, and the correlation matrix for the parameters have been deposited with the journal as supplementary data, and the PGOPHER input files (containing the constants derived below) have also been included for convenience.

3.1. $v' = 8$

The $v' = 8$ level of the $B\,^3\Sigma^-$ state is a good example of a straightforward analysis, since no significant perturbations were present in the spectra analysed. The available data comprised DFWM spectra of the (8,2) and (8,1) vibrational bands, and a plate absorption spectrum of (8,0). The linewidth and rotational temperature of the DFWM spectra were approximately 0.3 cm^{-1} and 300 K in both cases. The resolution of the absorption spectrum was lower ($\sim$2 cm^{-1}) but the spectrum extended to a higher J, reflecting a higher temperature ($\sim$600 K), so some assignments to (8,0) were included in the fit. Sample spectra and simulations are shown in Fig. 2, and constants derived from the analysis are given in Table 1. An excellent agreement between the experimental spectrum and simulation was noted, with an average error of approximately 0.05 cm^{-1} (much less than the laser linewidth), indicating no perturbations in $v' = 8$ of the B state.

A number of DFWM spectra of this and other bands were recorded at various distances between the photolysis and DFWM lasers, corresponding to different degrees of rotational cooling, and it was noted that a range of higher J'' lines were more intense than expected from a simple Boltzmann distribution. This was especially true for the DFWM spectra with less rotational cooling and was attributed to a non-Boltzmann population distribution within the initial X state. In the DFWM experiments, SO was produced by 193 nm photolysis of SO_2. Felder et al. [22] found that the average rotational energy of nascent SO fragments ($v' = 0$, 1, and 2) resulting from 193 nm photolysis is $\sim$30 rotational quanta, or 650 cm^{-1}. This provides an explanation of the appearance of the DFWM (8,2) spectrum in Fig. 2, where there is a local maximum in intensity around 43 700 cm^{-1}, corresponding to $J'' \sim 23$. The same effect is seen in the (5,1) spectrum shown in Fig. 3; this was recorded with less rotational cooling, and there is an increase in peak intensity as J increases beyond 43 135 cm^{-1}, peaking at $J \sim 28$.

3.2. $v' = 5$

An example of a vibrational level of the $B\,^3\Sigma^-$ state that is known to be affected by perturbations from other electronic states is $v' = 5$. Looking at the potential energy diagram (Fig. 1), there are a number of known bound electronic states lying in the same region as the $B\,^3\Sigma^-$ state, just above the first dissociation limit. The $C\,^3\Pi$ and $d\,^1\Pi$ are obvious candidates for interaction, and the most comprehensive analysis of these states is that of Archer et al. from a $1 + 1$ MPI study [15]. Within their analysis, an interaction between the $v' = 5$ level in the $B\,^3\Sigma^-$ state and the $v' = 0$ ($\Omega = 0$) level in the $C\,^3\Pi$ state was outlined. From an analysis of experimental MPI spectra of these two bands, a set of molecular constants and an interaction matrix element between the two states were derived. However, although the MPI spectrum of the (0,0) band of the C–X transition showed clearly resolved rotational structure with a linewidth of approximately 0.1 cm^{-1}, the (5,0) band of the B state only showed a weak and poorly resolved spectrum with a linewidth of $\sim$1 cm^{-1} (attributed to predissociation). In this previous work the four components ($\Omega = 2$, 1, 0^+ and 0^-) of the $C\,^3\Pi$ state were modelled separately as a considerable discrepancy in effective rotational constants was noted between components. This was attributed to their interaction with other states, including the B state. A simple deperturbation including the B and C states

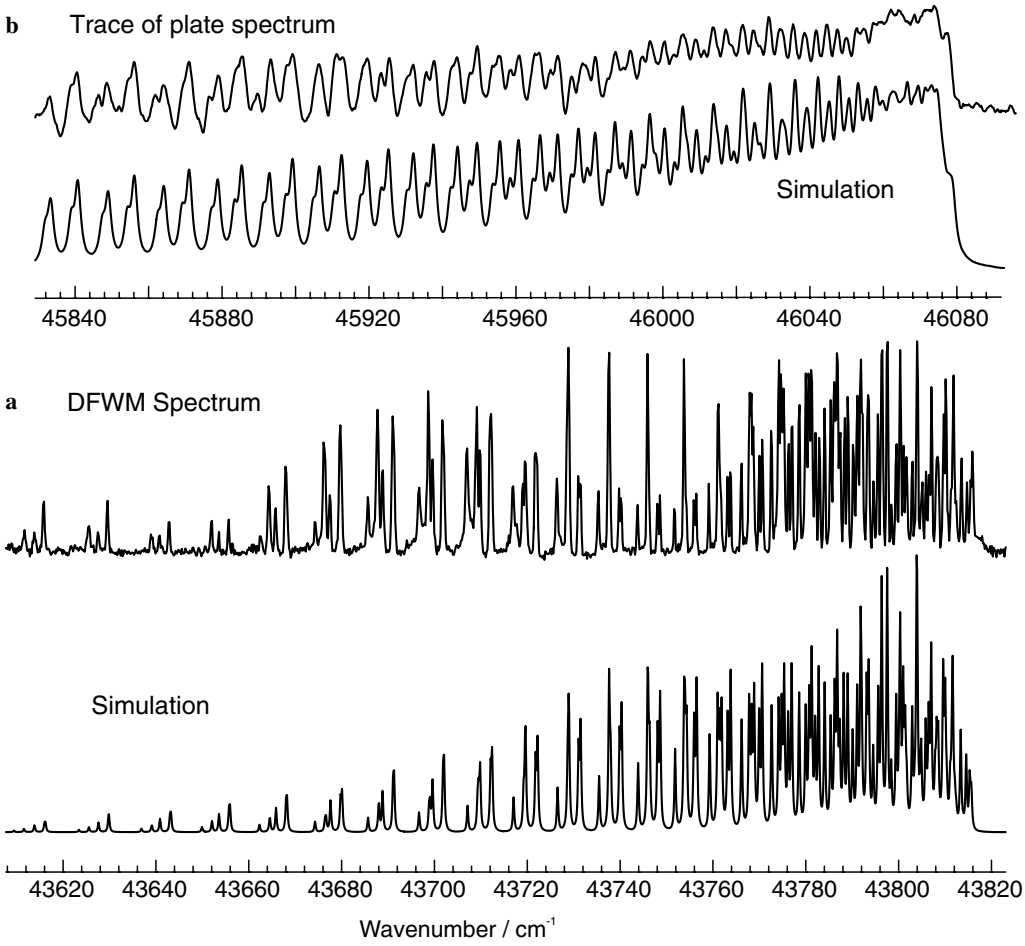

Fig. 2. Spectra and simulation of (a) DFWM spectrum of the (8,2) band of the B–X transition and (b) absorption spectrum of the (8,0) band. The absorption spectrum is a trace of a photographic plate. The anomalously high intensity in the centre of the DFWM spectrum arises from the non-Boltzmann distribution of the nascent SO.

could account for the difference in rotational constant between the 0^+ and 0^- components, and also explain discrepancies in simulated intensities. However, it was not possible to take the previous analysis further because of the poor resolution of the transitions to the B state. The DFWM spectra described here provide excellent information on $B\,v' = 5$, and allow a much better study of the interaction between the B and C states.

As for many of the other B state vibrational levels, a number of absorption and DFWM spectra were available for the analysis of $v' = 5$, covering the (5,0), (5,1), and (5,2) transitions. The present analysis concentrated on the DFWM spectrum of the (5,1) transition shown in Fig. 3, since this showed the best resolution ($\sim$1 cm^{-1}) and signal to noise ratio, and also extended to highest J.

The analysis of $v' = 5$ also included the (5,0) absorption spectrum, though the poorer signal to noise did not allow much extra information to be gained. Low temperature MPI spectra of Archer et al. [15] were also included in the analysis to provide information on the C and d states.

Initial analysis of the (5,1) band confirmed that the $v' = 5$ level is significantly perturbed. The deperturbation by Archer et al. predicted a crossing of the $\Omega = 0$ component of the lowest vibrational level of the $C\ ^3\Pi$ state with the $v' = 5$ level of the $B\ ^3\Sigma^-$ state at $J \sim 20$, though their experimental data only extended to $J = 9$. We therefore used this as a starting point for our analysis. Given this, assignment of the DFWM spectra was reasonably straightforward, confirmed by common differences using the ground state constants of Clerbaux and Colin [5] in most cases. The analysis revealed major perturbations in all three Ω components, at $J = 17$ (F1), $J = 21$ (F2), and $J = 27$ (F3).

To model the mixing between the B and C states, both a spin orbit operator and an L uncoupling operator were required. The spin orbit operator has selection rules $\Delta\Omega = 0$ and the parameter used is the following matrix element (in an unsymmetrised basis):

$$\langle C^3\Pi_1, v = 0|\hat{H}_{\mathrm{SO}}|B^3\Sigma_1^-, v = 5\rangle = \langle C^3\Pi_0, v = 0|\hat{H}_{\mathrm{SO}}|B^3\Sigma_0^-, v = 5\rangle \quad (2)$$

The L uncoupling has the conventional form:

$$-\beta(\hat{J}_-\hat{L}_+ + \hat{J}_+\hat{L}_-) \quad (3)$$

Table 1
Summary of constants (cm^{-1}) for the $B\ ^3\Sigma^-$ state of SO

v'	T_v	B	$D \times 10^{-6}$	λ	$\gamma \times 10^2$	Number of observations	Estimated linewidth	Perturbations	Data sources
0[a]	41 375.105(7)	0.498859(2)	1.294(2)	3.457(1)	−1.949(2)	—	—[b]	Several small, unidentified	(0,2) LIF, FT
1	41 991.97(1)	0.49426(9)	1.61(8)	3.20(2)	−1.37(9)	440	—[b]	See Table 3. $A\ ^3\Sigma^+\ v' = ?$, $A\ ^3\Pi\ v' = 10$, and other small	(1,1), (1,2) LIF, (1,6), (1,7) FT
2	42 599.04(2)	0.4589(7)	—	1.18(2)	3.7(3)	140	—[b]	Yes, Δ state, and others	(2,0), (2,2), (2,3) LIF
3	43 200.69(6)	0.465(1)	—	1.25(8)	2.4(8)	62	—[b]	Yes, unidentified	(3,2), (3,3), (3,4) LIF, (3,2) DFWM, (3,4) MPI
4	43 795.40(6)	0.4806(3)	4.3(3)	4.07(5)	−0.9(2)	148	<3	None	(4,0) abs, (4,2) DFWM
5	44 382.05(8)	0.4705(5)	−0.8(6)	1.0(1)	1.9(9)	238	<0.8	See Table 2. $C\ ^3\Pi\ v = 0$,$d\ ^1\Pi\ v = 1$	(5,0) abs, (5,1), (5,2) DFWM
6	44 954.76(8)	0.4678(7)	−9(1)	5.17(6)	0.85(3)	154	<1.2	None	(6,0) abs, (6.2) DFWM
7	45 524.0(7)	0.4612(5)	—	5.4(3)	—	155	<2	$C\ ^3\Pi\ v = 2$	(7,0) abs, (7,1) DFWM
8[c]	46 075.494(9)	0.45992(6)	1.39(7)	2.77(1)	−0.81(3)	362	<0.3	None	(8,0) abs, (8,1), (8,2) DFWM
9	46 624.59(4)	0.45024(7)	—	3.45(5)	−1.1(1)	244	<1.5	None	(9,0) abs, (9,1) DFWM
10	47 161.0(2)	0.447(1)	−2(1)	3.1(1)	−1.4(4)	73	<5	None	(10,0) abs
11	47 683.6(1)	0.4388(2)	—	4.8(2)	—	112	<1	$C\ ^3\Pi\ v = 5$	(11,0) abs
12	48 194.01(6)	0.4360(1)	—	2.89(7)	−1.2(2)	109	<7	None identified	(12,0) abs
13	48 691.6(1)	0.4329(5)	3.4(5)	2.31(7)	−1.9(2)	115	<10	None identified	(13,0) abs
14	49 935.7(5)	—	—	—	—	—	<20	Analysis not possible	(14,0) abs
15	49 708.3(5)	—	—	—	—	—	<40	Analysis not possible	(15,0) abs
16	50 049.9(3)	0.3822(6)	—	5.2(3)	—	133	<10	None identified	(16,0) abs

[a] Constants from reference [5].
[b] Below dissociation limit; linewidths expected to be below instrumental resolution (<0.1 cm^{-1}).
[c] $\lambda_D = 7.8\ (4) \times 10^{-4}\ cm^{-1}$.

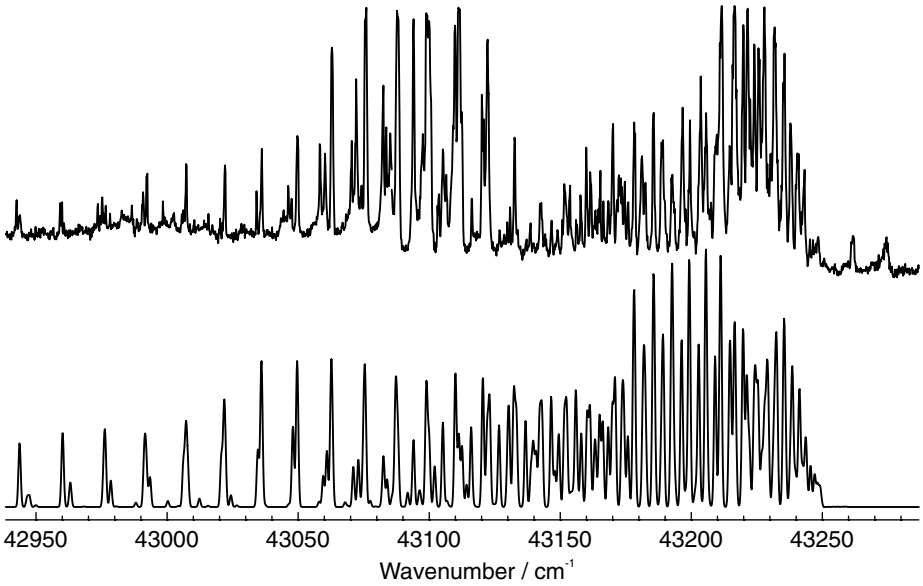

Fig. 3. DFWM experimental spectrum (upper trace) of the (5,1) band of the *B*–*X* transition, and simulation (lower trace). The effective temperature of the experimental spectrum is ~600 K. The anomalously high intensity in the centre of the spectrum arises from the non-Boltzmann distribution of the nascent SO.

and we define the parameter we use as the matrix element:

$$\langle C^3\Pi, v = 0, \Lambda = 1|\beta L_+|B^3\Sigma^-, v = 5\rangle \quad (4)$$

For the best fit we also had to allow for centrifugal distortion of these interactions, which take the form:

$$1/2\alpha_D\lfloor\hat{N}^2, \hat{H}_{SO}\rfloor_+ \quad (5)$$

$$1/2\beta_D\lfloor\hat{N}^2, \hat{J}_-\hat{L}_+ + \hat{J}_+\hat{L}_-\rfloor_+ \quad (6)$$

where $[A, B]_+ = AB + BA$. The parameters are defined by analogy with those in Eqs. (2) and (4).

A fit including just the $B\ v' = 5$ and $C\ v' = 0$ levels gave good results with this model for the interaction, but left a small but systematic discrepancy for the $C\ ^3\Pi_1$ component, which could only be fitted by using a slightly different effective *B* value for this component. Given the close proximity of $d\ ^1\Pi\ v' = 1$ this can be attributed to a mixing with this state. Inclusion of a spin-orbit mixing between these two states enabled a single rotational constant (0.567 (1) cm^{-1}) to be used to describe all Ω components of $C\ ^3\Pi\ v' = 0$, unlike in the previous work. The final Hamiltonian matrix used therefore included $B\ ^3\Sigma^-\ v' = 5$, $C\ ^3\Pi\ v' = 0$, and $d\ ^1\Pi\ v' = 1$, and the final constants from a fit to this Hamiltonian are presented in Table 2.

Given this model, a good fit to the *B*–*X* (5,1) vibrational band was obtained, as seen in Fig. 3. An energy level diagram, illustrating the crossing between the $B\ ^3\Sigma^-$ and $C\ ^3\Pi$ states is shown in Fig. 4. The diamonds and crosses represent "observed" *e* and *f* energy levels respectively, obtained by adding observed transition frequencies to the known ground state energy levels. From this diagram, it can be seen that there are some missing assignments at low *J*. During the fitting process, it was evident that some transitions around $J' = 9$ were displaced by up to 2 cm^{-1} from the model positions. The spectra we had were not clear enough to provide a detailed assignment of these transitions, but it is clear that there is another perturbation. However, assignment of the state causing this perturbation is not straightforward; the $C\ ^3\Pi$ and $d\ ^1\Pi$ states have already been accounted for, and none of the other bound states in Fig. 1 are in the right position to have an effect. The only states not included on the diagram are likely to be repulsive states correlating to the S (^1D) + O (^3P) dissociation limit. It is worth noting in this context that the $d\ ^1\Pi$ state is rather unusual and previous workers reported [15] that ab initio calculations performed on the $d\ ^1\Pi$ state were not easy to converge, with less accurate calculations giving a completely repulsive state. This could be the case for other states correlating with the first dissociation limit; the Wigner–Witmer rules allow us to confirm that the correct number of states have been included in the diagram but given the difficulty of the calculation, as illustrated by the $d\ ^1\Pi$ state, previous ab initio calculations could have missed a shallow well in one or more of these states. It is likely, therefore, that there is at least one formally repulsive state that is capable of supporting some bound levels, and this is most likely the source of the perturbation.

Table 2 also lists the parameters derived by Archer et al. [15] for comparison. Identical values are not to be expected given the differences in the models used, but it is clear that the single large spin orbit interaction of 16.61 (7) cm^{-1} found in the previous work has been split, giving a smaller interaction of 2.4 (4) cm^{-1}, accompanied by a significant *L* uncoupling perturbation. However, the previous work had to make several drastic assumptions because of the limited information available,

Table 2
Molecular constants for the $B\ ^3\Sigma^-\ v'=5$, $C\ ^3\Pi\ v'=0$, and $d\ ^1\Pi\ v'=1$ levels, and parameters resulting from a deperturbation of these states[a]

State	Parameter	Value[a]/cm^{-1}	Previous work[b]
$B\ ^3\Sigma^-\ v=5$	T_0	44382.05 (8)	44381.4 (3)
	B	0.4705 (5)	0.4755[c]
	λ	1.0 (1)	3.7[c]
	γ	−0.019 (9)	
	D	$-0.8\ (6)\times10^{-6}$	
$C\ ^3\Pi\ v=0$	T_0	44151.8 (3)	44336.28 (1)[d]
	B	0.567 (1)	0.5697 (2)
	A	−181.4 (1)	−179[c]
	λ	1.0 (4)	0[c]
	o	0.98 (8)	0[c]
	γ	−0.2 (1)	0[c]
	D	$1.2\ (2)\times10^{-5}$	0[c]
$d\ ^1\Pi\ v=1$	T_0	44143.2 (7)	44137.90 (1)
	B	0.626 (5)	0.6071 (4)
$\langle C^3\Pi_1, v=0 \mid \hat{H}_{SO} \mid B^3\Sigma_1^-, v=5\rangle$		2.4 (4)	16.61 (7)
$\langle C^3\Pi,\ v=0,\ \Lambda=1\vert\beta L_+\vert B\ ^3\Sigma^-,\ v=5\rangle$		0.32 (3)	—
$\langle C^3\Pi, v=0\vert\alpha_D\hat{H}_{SO}\vert B^3\Sigma^-, v=5\rangle$		0.0150 (9)	—
$\langle C\ ^3\Pi_0,\ v=0,\ \Lambda=1\vert\beta_D L_+\vert B\ ^3\Sigma^-,\ v=5\rangle$		$-4.1\ (5)\times10^{-4}$	—
$\langle C^3\Pi, v=0\vert\hat{H}_{SO}\vert d^1\Pi, v=1\rangle$		8.7 (3)	—

[a] Figures in parentheses are one standard deviation.
[b] Reference [15].
[c] Fixed at assumed value.
[d] Value not directly comparable—this is the effective origin of the $^3\Pi_0$ component.

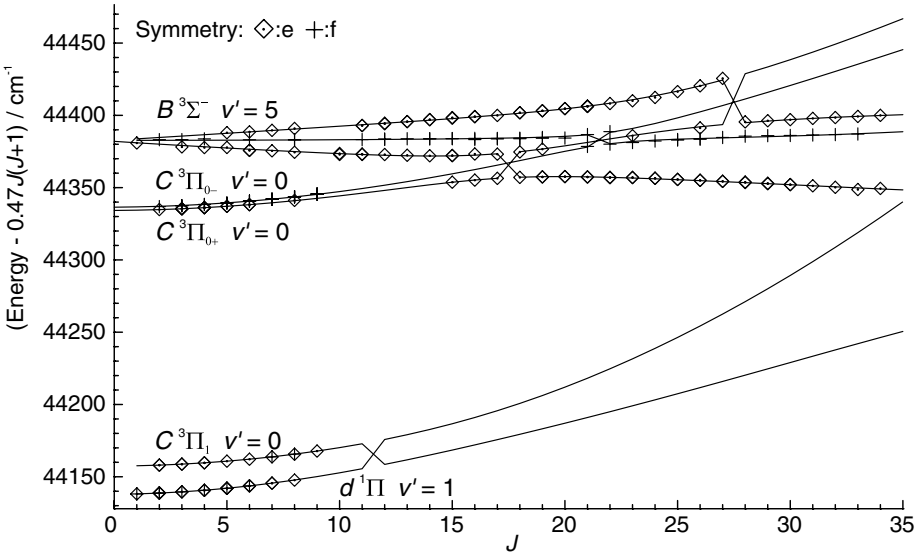

Fig. 4. Energy level diagram showing observed and calculated upper state reduced term values (term value, $-0.47J(J+1)$) plotted against J for $B\ ^3\Sigma^-$ state $v'=5$, $C\ ^3\Pi$ state $v'=0$ ($\Omega=2$ is off the bottom of the diagram), and $d\ ^1\Pi$ state $v'=1$, showing mixing between the states. The diamonds and crosses represent "observed" e and f energy levels obtained by adding observed transitions to calculated ground state energy levels.

including that the Λ doubling in the $C\ ^3\Pi_0$ component was entirely due to the nearby B state. This work does not have to make this assumption, and a significant Λ doubling constant (o) of 0.98 (8) cm^{-1} is determined. Given this and other assumptions in the previous work, any discrepancies are unsurprising.

Ab initio off-diagonal spin-orbit matrix elements between the C and d states, and also between the B and C states, are available from Figure 6 of Reference [15]. Averaging over approximate vibrational wavefunctions indicated a value of 12.95 cm^{-1} for the matrix element $\langle C^3\Pi, v=0\vert\hat{H}\vert B^3\Sigma^-, v=5\rangle$. Comparing this with our measured value of 2.4 (4) cm^{-1} suggests that the ab initio calculations are at least qualitatively right. A calculated $\langle C^3\Pi, v=0\vert\hat{H}_{SO}\vert d^1\Pi, v=1\rangle$ matrix element of ~40 cm^{-1} is also available. This could well be consistent

with our measured value of 8.7 (3) cm^{-1}, when the overlap between vibrational wavefunctions is taken into account.

3.3. $v' = 1$

The analysis of $B\ v' = 1$ was also complicated by a number of perturbations. A partial rotational analysis of this level had been previously attempted by Clerbaux and Colin [5]. A fit to the (1,5), (1,6), and (1,12) bands of a $B\ ^3\Sigma^- – X\ ^3\Sigma^-$ Fourier transform emission spectrum had enabled a rotational analysis between $J' = 10–53$. Several perturbations were evident, though each one only affected a few rotational levels.

Here, a more complete analysis of the $v' = 1$ level of the $B\ ^3\Sigma^-$ level has been achieved, particularly at low J. Again, spectra from a number of different sources were used. These comprised the Fourier transform spectrum used for the earlier analysis in Reference [5], and LIF spectra of the (1,2) and (1,3) bands. Analysis of the low temperature LIF spectra (15–100 K) in conjunction with the Fourier transform spectrum (~1400 K) extended to $J = 55$ and including the low J levels for the first time. A number of perturbations within $v' = 1$ were noted. One of these, at $J = 28$ (F1), can be attributed to a crossing with the now known $\Omega = 1$ component of $A\ ^3\Pi\ v' = 10$, and was modelled using an L uncoupling operator as for $B\ v' = 5$. In addition, a number of perturbations were noted at lower J, as shown in Fig. 5. The pattern of displaced lines in the e and f components of $B\ v' = 1$, between $J = 5–10$, is such that the perturbation can be modelled by a single $^3\Sigma^+$ state. One SO $^3\Sigma^+$ state that tends to the first dissociation limit is known; $A''\ ^3\Sigma^+$. However, there is very little information available about this state. Ab initio studies by Dixon et al. [23] and Swope et al. [24] proved its existence, and an experimental observation of some part of the emission spectrum of the $A''\ ^3\Sigma^+ – X\ ^3\Sigma^-$ transition was recently observed [13], but the experimental data only extends to $v' = 4$. A simple extrapolation of vibrational levels suggests we are observing $v' = 14$.

It was found that, on increasing the laser power whilst recording LIF spectra of the (1,2) band, some extra peaks that could not be assigned to the $B–X$ transition were observed. As the $B–X$ transition saturates, a number of other peaks appear over a range of 15 cm^{-1} to a slightly higher wavenumber than the $B–X$ (1,2) vibrational band. While we did not make quantitative measurements, the lifetimes of the levels populated by these transitions is slightly longer than those of the B state but much less than that of the $A\ ^3\Pi$ state. Detailed modelling in PGOPHER allowed the majority of the extra peaks to be assigned to the $^3\Sigma^+$ state. To model the perturbation between the B and A'' states, both a spin orbit operator and an S uncoupling operator were used, where the S uncoupling takes the form

$$-\beta(\hat{J}_+ S_- + \hat{J}_- S_+) \tag{7}$$

which we take as having matrix elements in an unsymmetrised basis of

$$\langle A''^3\Sigma^+, v = ?, \Sigma = 1 | \beta S_+ | B^3\Sigma^-, v = 1, \Sigma = 0 \rangle = \sqrt{2}\sqrt{J(J+1)}\beta \tag{8}$$

Fig. 5 shows an energy level diagram for $B\ v' = 1$, showing the crossings of both the $\Omega = 1$ component of $A\ v' = 10$, and of some vibrational level of the $A''\ ^3\Sigma^+$ state. "Observed" e and f energy levels for these three states are indicated using diamonds and crosses, as before. Other small perturbations within $B\ v' = 1$ were

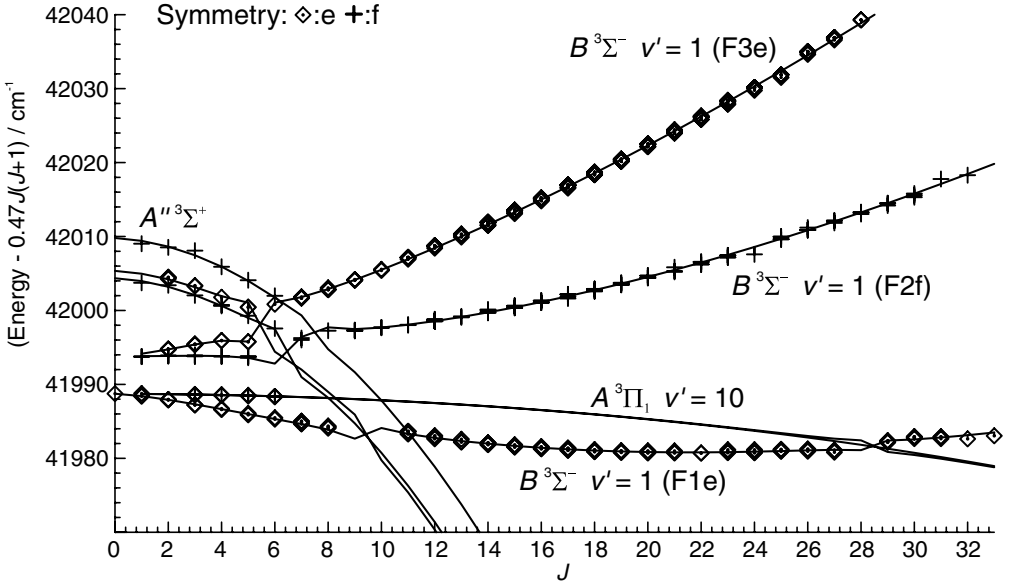

Fig. 5. Energy level diagram showing observed and calculated upper state reduced term values (term value, $-0.47J(J+1)$) plotted against J for $B\ ^3\Sigma^-$ state $v' = 1$, $A\ ^3\Pi$ state $v' = 10$ ($\Omega = 0$) and some vibrational level of the state assumed to be $A''\ ^3\Sigma^+$.

Table 3
Molecular constants for the $B\ ^3\Sigma^-$ $v'=1$, $A\ ^3\Pi$ $v'=10$ levels and a vibrational level of $A''\ ^3\Sigma^+$ (probably $v'=14$) and parameters resulting from a deperturbation of these states

State	Parameter	Value[a]/cm^{-1}
$B\ ^3\Sigma^-$ $v=1$	T_0	41991.97 (1)
	B	0.49426 (9)
	λ	3.20 (2)
	γ	$-1.37\ (9)\times10^{-2}$
	D	$1.61\ (8)\times10^{-6}$
$A\ ^3\Pi$ $v=10$	T_0	41990.00 (4)
	B	0.4618 (5)
	A	134.86 (5)
	λ	1.67 (4)
	o	0.45 (8)
	D	4×10^{-7}[b]
$A''\ ^3\Sigma^+$	T_0	42007.35 (9)
	B	0.256 (3)
	λ	−2.66 (6)
	γ	0.81 (3)
$\langle A^3\Pi_1, v=10, \Lambda=1 \mid \beta L_+ \mid B^3\Sigma_1^-, v=1\rangle$		−0.020 (3)
$\langle A''^3\Sigma^+ \mid \hat{H}_{SO} \mid B^3\Sigma^-, v=1\rangle$		1.87 (4)
$\langle A''^3\Sigma^+ \mid JS \mid B^3\Sigma^-, v=1\rangle$		−0.161 (4)

[a] Figures in parentheses are one standard deviation.
[b] Fixed value.

noted at higher J as in the previous analysis, but the source of these has not been identified. There are, however, several states in the region that could account for these, as can be seen from Fig. 1.

The final Hamiltonian matrix used therefore included $B\ ^3\Sigma^-$ $v'=1$, $A\ ^3\Pi$ $v'=10$, and one vibrational level of $A''\ ^3\Sigma$. Final constants from a fit to this Hamiltonian are given in Table 3.

3.4. Other levels

A summary of all molecular constants determined from analysis of vibrational levels up to $v'=16$ is given in Table 1. Rotational analysis of $v'=0$ level of the $B\ ^3\Sigma^-$ state is relatively straightforward, and a comprehensive study of this band has been carried out previously by Clerbaux and Colin [5], from fitting to the (0,6), (0,7), (0,8), (0,9), (0,10), (0,11), and (0,12) bands of the $B\ ^3\Sigma^-$–$X\ ^3\Sigma^-$ Fourier transform emission spectrum. A number of perturbations were observed, especially at higher J. Identification of these perturbations has not yet been achieved, as each of these only involves a few rotational levels so little information is available about the perturbing state.

Several B state vibrational levels, in addition to $v'=8$, were found to be completely unperturbed. These are $v'=4$, 6, 9, and were analysed using a combination of DFWM and absorption spectra.

Analysis of $v'=2$ and $v'=3$ has not been achieved beyond the lowest J. Given that these levels are just below the first dissociation limit, a high density of states and therefore perturbations is to be expected for these levels. It is evident from the LIF spectra of various hot bands available that there are significant perturbations affecting both these levels. Acquisition of LIF spectra for both of these levels, using a higher laser power, caused saturation and revealed extra peaks not attributable to the B state, as for $v'=1$. Again, these peaks do not match with the known A, C, or d states. The extra structure seen in the region of $v'=2$ could be fitted as an $\Omega=2$ state, and could thus be attributed to either the $A'\ ^3\Delta$ or the $a\ ^1\Delta$ state, but no further conclusions can be reached. A simple fit (ignoring interactions between states) to a $^1\Delta$ state yielded $T_v=42\,630.86\ (4)$, $B=0.314\ (1)$ cm^{-1}. In any case, it is evident from the number and position of perturbations in $v'=2$ that there is at least one other, unidentified, state interacting with this level. The extra structure associated with the $v'=3$ level could not be assigned to any specific electronic state, but it is clear that $v'=3$ is very perturbed.

Another band which proved difficult to analyse is $v'=7$. From the (7,0) absorption band, it is clear that this band is perturbed as extra features are found near the (7,0) band head, at term values of $T_v=46\,099$, 46 104, 46 109, 46 123, and 46 132 cm^{-1}. These are very likely due to an interaction with a component of the so far unobserved $C\ ^3\Pi$ $v'=2$. Above $v'=1$, nothing is experimentally known about the C state, but, according to theoretical constants calculated by Ornellas and Borin [16], the C $v'=2$ level is predicted to lie somewhere in the region of B $v'=7$. The poor resolution of the (7,0) absorption spectrum only allowed an approximate fit to be achieved, with B state constants as given in Table 1, C state constants of $T_v=45518\ (2)$ cm^{-1}, $B=0.566\ (2)$ cm^{-1} and $A=-181.4$ cm^{-1} (fixed), and a $\langle C^3\Pi_1, v=2|\hat{H}_{SO}|B^3\Sigma_1^-, v=7\rangle$ matrix element of 16 (1) cm^{-1}. Attempts to record a DFWM spectrum of (7,2) failed, since it is almost completely obscured by the (5,1) band. This is counter-intuitive, since a consideration of DFWM transition intensities indicates that (7,2) should be significantly more intense than (5,1). However, almost all the structure in the region of (5,1) and (7,2) can be assigned to (5,1), and the correctness of these assignments confirmed by the corresponding fits to (5,2) and (5,0). The DFWM spectrum of the (7,1) is of poor quality and was impossible to analyse. It should however be mentioned that the extra features found near the (7,0) band head are also observed near the (7,2) and (7,1) band heads.

Beyond $v'=9$, data available for analysis was reduced, due to small DFWM transition intensities. For $v'=11$, a poor (11,2) DFWM spectrum was obtained, but was overlapped by (9,0). A rough fit to the (11,0) absorption spectrum was attempted, which indicated some perturbations within $v'=11$. The only known state at an appropriate energy to interact with this B vibrational level is $C\ ^3\Pi$. According to the calculations of Ornellas and Borin [16], the $v'=5$ level of the C state is predicted to lie near B $v'=11$, so it can be assumed that the C state is causing the perturbations observed in (11,0), although we have not enough information to carry out a deperturbation.

$v'=10$, 12, and 13 have been analysed using absorption spectra alone, and appear to be essentially unperturbed.

Beyond $v' = 13$, the absorption spectra become very diffuse, and identification and assignment of rotational lines becomes impossible, with the exception of $v' = 16$.

3.5. Linewidths

Table 1 includes estimated linewidths derived simply by comparing simulations at various linewidths for transitions within each vibrational level of the B state. We have not checked for a power dependence of these widths, and have not modelled the DFWM lineshapes in detail, so these should be considered as rough upper limits only. For the levels that lie below the first dissociation limit ($v' = 0$, 1, 2, and 3), the linewidths are assumed to be instrument limited. For levels above the first dissociation limit, linewidths are taken from DFWM spectra, where available, otherwise from the lower resolution absorption spectra. Even given the limitations in the measurements, there is a clear variation in linewidth between vibrational levels. There is a definite increase in linewidth around $v' = 9$, and an even more noticeable increase around $v' = 14$, and $v' = 15$, for which rotational structure cannot be resolved. Rotational structure is clear in $v' = 16$ but not for any higher vibrational level. On the other hand, there is no evidence of a variation with spin state or J, suggesting a homogeneous mechanism. The origins of these variations in linewidth can be attributed to crossings with other repulsive electronic states. The potential energy diagram in Fig. 1 suggests that there are two repulsive states that could be responsible for the increased linewidth at $v' = 9$, and there are several other repulsive states crossing at higher energy that can account for the increase in linewidth around $v' = 14$ and $v' = 15$. Even with our limited precision on the linewidth, we can see that while the overall trend is increasing linewidth with v' the variation is not monotonic, which possibly reflects interference between the possible channels for dissociation.

4. Conclusion

We have performed a detailed rotational analysis and deperturbation of the vibrational levels within the $B\ ^3\Sigma^-$ state of SO up to $v' = 16$, using spectra from a wide range of sources. In a number of cases we have been able to identify the origin of perturbations seen within the $B\ ^3\Sigma^-$ state; perturbing states identified include the $A\ ^3\Pi$, $C\ ^3\Pi$, $d\ ^1\Pi$, and $A''\ ^3\Sigma^+$ states, and there is no doubt that other nearby electronic states are also responsible for interactions with the B state. A clearer understanding of the interactions between states enables a clearer picture of the spectroscopy of SO to be formed.

Acknowledgments

We are pleased to thank the Belgian National Fund for Scientific Research (FRFC Convention), the Communauté française de Belgique (Action de Recherches Concertées), the National Science Council of Taiwan (Project Nos. NSC94-2113-M-009-004 and NSC95-2113-M-009-002) and the Engineering and Physical Sciences Research Council (UK) for funding.

Appendix A. Supplementary data

Supplementary data for this article are available on ScienceDirect (www.sciencedirect.com) and as part of the Ohio State University Molecular Spectroscopy Archives (http://msa.lib.ohio-state.edu/jmsa_hp.htm).

References

[1] E.V. Martin, Phys. Rev. 41 (1932) 167–193.
[2] G. Norrish, G.A. Oldershaw, Proc. R. Soc. (London), Ser. A 249 (1959) 498–512.
[3] J.J. McGarvey, W.D. McGrath, Proc. R. Soc. (London), Ser. A 278 (1963) 490–504.
[4] R. Colin, Can. J. Phys. 47 (1969) 979–994.
[5] C. Clerbaux, R. Colin, J. Mol. Spectrosc. 165 (1994) 334–348.
[6] J.M.F. Elks, C.M. Western, J. Chem. Phys. 110 (1999) 7699–7706.
[7] M. Bogey, S. Civiš, B. Delcroix, C. Demuynck, A.F. Krupnov, J. Quiguer, M.Y. Tretyakov, A. Walters, J. Mol. Spectrosc. 182 (1997) 85–97.
[8] R. Colin, Can. J. Phys. 46 (1968) 1539–1546.
[9] M. Wong, T. Amano, P. Bernath, J. Chem. Phys. 77 (1982) 2211–2213.
[10] H. Kanamori, J.E. Bulter, K. Kawaguchi, C. Yamada, E. Hirota, J. Mol. Spectrosc. 113 (1985) 261–624.
[11] C.-C. Zen, F.-T. Tang, Y.-P. Lee, J. Chem. Phys. 96 (1992) 8054–8061.
[12] Y. Chu, H. Wang, J. Li, P. Cheng, D. Cao, Chem. Phys. Lett. 366 (2002) 147–152.
[13] H.M. Wang, X.S. Tang, S.K. Zhou, W.J. Zhang, Y.A. Chu, Chem. Phys. Lett. 407 (2005) 78–82.
[14] R. Colin, J. Chem. Soc., Faraday Trans. 78 (1982) 1139–1147.
[15] C.P. Archer, J.M.F. Elks, C.M. Western, J. Chem. Phys. 112 (2000) 6293–6300.
[16] F.R. Ornellas, A.C. Borin, Mol. Phys. 94 (1998) 139–145.
[17] W.-C. Hung, M.-L. Huang, Y.-C. Lee, Y.-P. Lee, J. Chem. Phys. 103 (1995) 9941–9946.
[18] A. Kumar, C.-C. Hsiao, Y.-Y. Lee, Y.-P. Lee, Chem. Phys. Lett 297 (1998) 300–306.
[19] K. Yamasaki, F. Taketani, S. Kazuyuki, I. Tokue, K. Tsuchiya, J. Phys. Chem. A 108 (2004) 2382–2388.
[20] PGOPHER, a Program for Simulating Rotational Structure, C. M. Western, University of Bristol, <http://pgopher.chm.bris.ac.uk/>.
[21] MOLPRO, a package of ab initio programs designed by H.-J. Werner and P. J. Knowles, version 2002.1, R. D. Amos, A. Bernhardsson, A. Berning, P. Celani, D. L. Cooper, M. J. O. Deegan, A. J. Dobbyn, F. Eckert, C. Hampel, G. Hetzer, P. J. Knowles, T. Korona, R. Lindh, A. W. Lloyd, S. J. McNicholas, F. R. Manby, W. Meyer, M. E. Mura, A. Nicklass, P. Palmieri, R. Pitzer, G. Rauhut, M. Schütz, U. Schumann, H. Stoll, A. J. Stone, R. Tarroni, T. Thorsteinsson, and H.-J. Werner.
[22] P. Felder, B.-M. Haas, R. Huber, Chem. Phys. Lett. 204 (1993) 248–256.
[23] R.N. Dixon, P.W. Tasker, G.G. Balint-Kurti, Mol. Phys. 34 (1977) 1455–1471.
[24] W.C. Swope, Y.-P. Lee, H.F. Schaefer, J. Chem. Phys. 71 (1979) 3761–3789.